Alireza Ashrafian

Numerical investigation of turbulent flow in a channel with rough walls

Department of Energy and Process Engineering
Norwegian University of Science and Technology
Trondheim, Norway, 2004

Dedicated to the
memory of my father,
Ashraf Ashrafian.

Table of Contents

Synopsis

This thesis presents a study of turbulent flow at low Reynolds number in a straight channel with rough walls using direct numerical simulation. It consists of two main parts. Part one contains several chapters on the theories associated with the subject and the numerical simulation. Part two presents results obtained from this study in the form of four self-contained articles and one conference paper as follows:

Article I

Ashrafian, A., Andersson, H. I. & Manhart, M., 2004 'DNS of turbulent flow in a rod-roughened channel', published in the *International Journal of Heat and Fluid Flow*, Vol. 25, pp. 373–383.

Article II

Ashrafian, A. & Andersson, H. I., 2004 'The structure of turbulence in a rod-roughened channel', submitted to the *International Journal of Heat and Fluid Flow*.

Article III

Ashrafian, A. & Andersson, H. I., 2004 'Roughness effects in turbulent channel flow', resubmitted to the *International Journal of Progress in Computational Fluid Dynamics*.

Article IV

Ashrafian, A., Bakken, O. M., Krogstad, P.-Å., & Andersson, H. I., 2004 'Rough-wall turbulence – a comparative study', published in *Advances in Turbulence X, Proceedings of the 10th European Turbulence Conference*, editors: H. I. Andersson and P.-Å. Krogstad, Trondheim, Norway, 29 June–2 July, pp. 293–296, a publishing of CIMNE, Barcelona.

Article V

Krogstad, P.-Å, Andersson, H. I., Bakken, O. M. & Ashrafian, A., 2004 'An experimental and numerical study of channel flow with rough walls', resubmitted to the *Journal of Fluid Mechanics*.

Abstract

Direct numerical simulation has been performed in order to study pressure-driven turbulent flow in a rod-roughened channel at Reynolds number $Re_\tau = 400$ (based on the mean pressure gradient). Square rods were attached to both channel walls and protruded only 0.034 of the channel's half-height into the flow. Roughness elements were spaced at 7 heights, which corresponded to the so-called "k–type" laboratory roughness.

The classical logarithmic variation of the mean velocity was found to be maintained in the rough-wall channel flow. The only effect roughness had was to shift the log-profile downwards, the magnitude of which was about 7.1. This, corresponded to the upper limit of the *transitionally rough* region, based on the associated equivalent sand-grain roughness height. Within the layer of thickness about 3-5 times roughness height (*roughness sublayer*), the dependency of the mean velocity and turbulence properties on the streamwise location with respect to the rods was revealed.

Instead of viscous sublayer, an intensive shear layer was formed emanated from the crest of roughness elements. It was observed that the wall-ward transport of the kinetic energy was substantially increased very close to the wall while the transport of the kinetic energy away from the wall was relatively reduced at just about the edge of the roughness sublayer. Visualizations of the fluctuating velocities and vortices in this region revealed the presence of elongated streaky structures very similar to those routinely observed in the structure of the smooth-wall turbulence, with much shorter coherence in the streamwise direction and less organization in the spanwise direction. The intensity of the vorticity fluctuations in the roughness sublayer were increased whereas in the outer layer, they remained unaffected. The anisotropy invariant maps for the smooth and rough cases clearly showed that the state of the near-wall turbulence for the two cases were substantially different, whereas in the regions away from the wall, the two cases exhibited similarities. Generally, the results obtained from this study supported the classical wall similarity hypothesis.

Acknowledgements

This work has been carried out over a three years period of PhD studies at the Norwegian University of Science and Technology. Despite being short, this period gave me a handful of life experience, knowledge and frequent opportunities. I am most grateful to the Research Council of Norway for granting a research fellowship that made my stay in Trondheim gracious.

I owe a good deal to many great people. Surely, I owe the most to my supervisor, professor Helge I. Andersson, who was remarkably supportive in any aspect of my work. Quite sadly, I lost my beloved father during the course of this work after that he underwent a tragic accident. Had I not received my supervisor's support, I would have never been able to be with my father and my family at the time that I needed them and they needed me. I should thank Prof. Andersson also for his exceptional attitude towards research and for his advice on the articles resulted from this study.

I owe a special dept of thanks to my co-supervisor, Prof. Per-Åge Krogstad and my fellow, Dr. Ole M. Bakken, for their motivation and inspiring discussions during the course of this work. Peter S. Johansson receives special thanks for the fruitful discussions and the share of frustration resulted from the "turbulence" that often dominated our minds. Together with other friends, our long excursions in the unique countryside of Norway were always soothing. Special thanks to Petter A. Berthelsen with whom sharing the office was most cheerful, and Reidar Kristoffersen who made such a friendly atmosphere for our group. I should also appreciate the administrative staff, Gerd R. Fremstad and Ingrid Wiggen, for their kindness and high level of performance.

Finally, I thank my friends, Hamed Miri and Marco Semini, with whom I spent such a joyful time in the Moholt Student Village, and my friends of all times, Vahid and Azi for their kindness. Special thanks go to Vigdis Winnberg for her extraordinary help and support during the period of writing up this thesis.

Alireza Ashrafian
Trondheim, August 2004

Part One

Johann Nikuradse (1894-1979)

Chapter 1

Introduction

Surface roughness has long been recognized as having a substantial effect on the flow resistance, be it as increased skin friction in an external flow or as increased pressure loss in an internal flow. It is not wholly in the wrong if we state that the advent of turbulence research finds itself in the surface roughness. It was not known until the experiments in 1800 by Coulomb (Rouse & Ince (1957)) that surface roughness has an effect on friction resistance. A German engineer named Hagen (1854) first reported that there might be two regimes of viscous flow in the pipe as he observed a sudden increase in the pressure drop by increasing the mass flow rate. It was shortly after Hagen that a French engineer, Darcy (1857) particularly motivated the rough-wall turbulence research by his pipe-flow experiments. The sole problem of finding the head loss in the pipe flow was to correlate the wall friction with flow conditions.

In this chapter a short review on early rough-wall boundary layer research is presented. Roughness classification and in particular, issues concerning the two-dimensional rod roughness are addressed.

1.1 Classical fluid mechanics

Darcy introduced the *friction factor*

$$f = \frac{8\tau_w}{\rho \overline{U}^2}, \tag{1.1}$$

as a constant of proportionality between the shear stress at the wall, τ_w, and the inertial force of the fluid. $\overline{U}$ is the bulk fluid velocity of the fluid. In 1883, Osborne Reynolds, a British engineering professor, introduced his non-dimensional parameter $Re_d = \overline{U}d/\nu$ to the community and claimed that its value was responsible for the sudden increase of pressure drop in the pipe flow at different volumetric flow rates.

ν is the kinematic viscosity of the fluid and d, is the diameter of the pipe. He introduced a dye streak into a pipe flow and observed transition and turbulence. The laminar velocity distribution in pipe is called *Hagen-Poiseuille flow* for which the Darcy friction factor is,

$$f = \frac{64}{Re_d}. \tag{1.2}$$

Ludwig Prandtl (1875-1953), the German engineering genius, introduced the *boundary layer theory* in 1904 (Prandtl, 1904). One of his earliest students, Paul R. H. Blasius, provided a mathematical basis for boundary-layer drag and showed as early as 1911 that the resistance to flow through smooth pipes could be expressed in terms of the Reynolds number for both laminar and turbulent flows. His phenomenal formula is the first correlation ever made for the turbulent pipe flow, between the friction factor and the Reynolds number,

$$f = 0.316 Re_d^{-1/4}. \tag{1.3}$$

Although his formula could finally explain Hagen's data after nearly 70 years, his supervisor was not very happy with it because of its limited range of application ($4000 < Re_d < 10^5$). [1]

Prandtl left the issue of evaluating the friction factor in rough-wall pipes to his other student, Johann Nikuradse (1894-1979) who performed his classical measurements in rough pipes. Nikuradse (1933) took a number of smooth pipes of diameter 2.5, 5 and 10 cm, and tightly coated the inside walls with uniform grains of graded sand from the Göttingen region of Germany. The *relative roughness* of each tube was then defined as ϵ/d, where ϵ was the diameter of the sand grains and d the diameter of the tube. The advantages of dimensionless numbers had been well learned from Osborne Reynolds. Nikuradse took pressure drop and velocity profile measurements in the pipes and obtained the corresponding $f - Re_d$ graphs which are illustrated on Figure 1.1. The range of the relative roughness was $0.002 \leq \epsilon/d \leq 0.06$.

Nikuradse observed that at low Reynolds numbers the laminar friction factor correlation is valid irrespective of the grain size. However, turbulent friction correlation, after an onset point, increases monotonically with ϵ/d. For any given relative roughness, the friction factor eventually becomes constant at higher Reynolds numbers. Based on these observations, Nikuradse introduced the roughness Reynolds number $\epsilon^+ = \epsilon u_\tau/\nu$ in order to characterize the observed behavior of turbulent flow in rough pipes. Whereas ϵ is a geometrical quantity, ϵ^+ is a *flow quantity*.

[1] Prandtl (1935) himself derived, $f^{-1/2} = 1.99 \log\left(Re_d f^{1/2}\right) - 1.02$, from the logarithmic mean-velocity profile (cf. Chapter 2). This correlation is quite recently corrected by McKeon et al. (2004) using data from the Princeton "superpipe" for $300,000 < Re_d < 36,000,000$. The new correlation is $f^{-1/2} = 1.930 \log\left(Re_d f^{1/2}\right) - 0.537$.

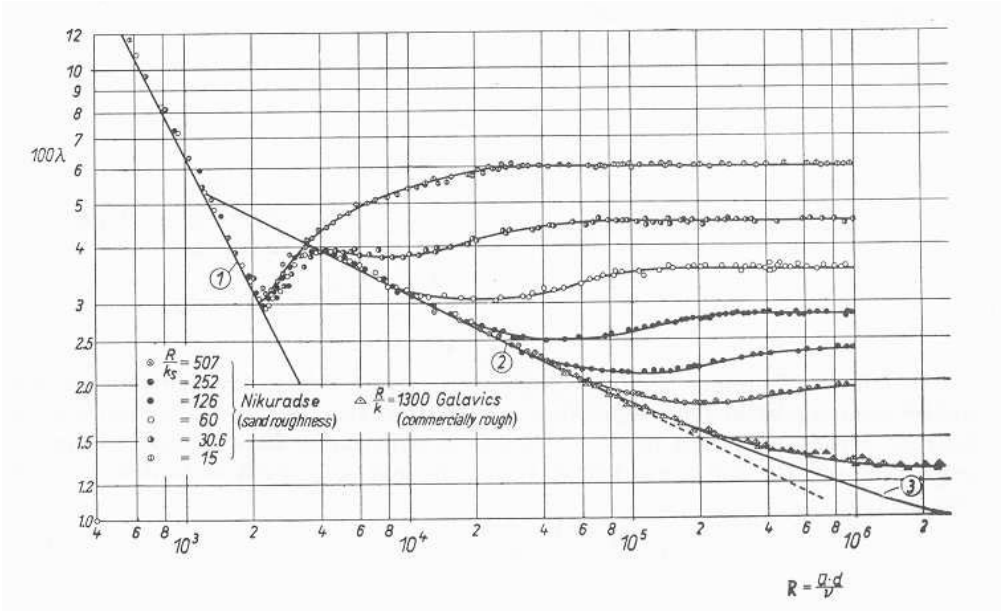

Figure 1.1: The friction factor (λ) vs. Reynolds number (R) diagram resulted from the experiments with sand-grain roughness by Nikuradse (1933). The figure is taken from Schlichting (1968).

The hypothesis of the existence of a boundary layer assisted Nikuradse to explain the behavior of the curves in Figure 1.1. At the walls, there can be no cross velocities except on a molecular scale. Hence, there must be a thin layer close to each wall through which the velocity increases from zero (actually at the wall) to some finite velocity sufficiently far away from the wall for an *eddy* to exist. Although this viscous layer is very thin, it has a marked effect on the behavior of the total flow in the pipe. All real surfaces (even polished ones) have some degree of roughness. If the peaks of the roughness do not protrude through the *viscous sublayer* ($\epsilon^+ < 7$) then the surface may be described as *hydraulically smooth* and the wall resistance is limited to that caused by viscous shear within the fluid. On the other hand, if the asperities protrude well beyond the viscous sublayer, then the disturbance that they introduce to the flow will cause additional eddies to be formed, consuming mechanical energy and resulting in a higher resistance to the flow. Moreover, as the velocity and, hence, the Reynolds Number increases, the thickness of the viscous sublayer decreases such that the turbulent flow fully triggers the irregularities on the surface of the wall at almost any scale. Any given pipe will then be *hydraulically rough* if roughness projects well beyond the viscous sublayer ($\epsilon^+ > 70$). Between

the two conditions there will be a *transition zone* ($7 < \epsilon^+ < 70$) where some, but not all of the surface irregularities protrude through the viscous sublayer.

Following Nikuradse's work, the other student of Prantl, Hermann Schlichting (1936) argued that in many practical applications, the density of the wall roughness is considerably smaller such that it can no longer be only described by the relative measure of ϵ/d. Schlichting's studies on the effects of "technical" roughness on the flow resistance has remained the cornerstone of the flow measurements over well-defined rough surfaces. He proposed the concept of *equivalent sand-grain roughness* as a viable measure of the flow-resistance character of a rough surface.

Based on Nikuradse's comprehensive data, Schlichting considered sand grain as *standard roughness*. For an arbitrary roughness shape merged into a turbulent flow at certain Reynolds number, the equivalent sand-grain roughness, k_s, is the sand-grain size that gives the same flow resistance at the same flow Reynolds number. The equivalent sand-grain roughness is simply an attempt to model a complex phenomenon with only a single parameter, i.e., the roughness height. A general requirement is that flow resistance data must be available in order to determine the equivalent sand-grain roughness height for a given surface. Schlichting was indeed aware of fitting the data obtained from commercially rough surfaces into the scale of sand roughness. He mentioned, for example, a peculiar type of roughness which gave very large values of resistance coefficient. This roughness shape was a rod-like deposit formed naturally at right angles to the flow direction. The height of the deposit was about 0.5 mm and the pipe diameter was 500 mm, giving $\epsilon/d \simeq 0.001$. Despite the small value of ϵ/d, the effective sand roughness was about 30 times the height of the deposited rods. Therefore, it was concluded that rod-like configuration lead to much higher resistance than sand roughness of the same absolute diameter. It might be supposed that normal boundary layer theory and its consequences would be violated by so great a relative roughness, but this did not deter Schlichting from applying the equivalent sand-grain roughness theory, nor has it deflected other practitioners from following him.

Further experiments and analytical investigations to derive a resistance formula for rough pipes were carried out in England by Colebrook (1938) in the late 1930's and followed by an engineer from Princeton, Lewis F. Moody (1944). Moody's landmark paper appeared after those of Nikuradse and Schlichting and represented the first easily applied and universally accepted method of comparing flow resistance for fully developed flow in commercially-rough pipes. It is probably the most famous and useful figure in the fluid mechanics (White, 1999).

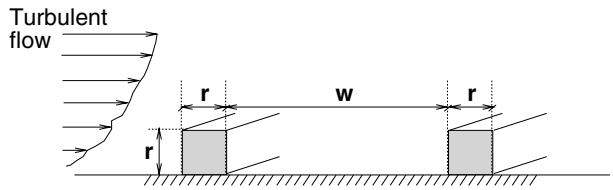

Figure 1.2: Schematic of a k–type rod roughness configuration.

1.2 Laboratory roughness classification

The large difference between the effects of sand-grain roughness and those of other arbitrary roughness distributed rather sparsely on the wall, reinforces the need for studying particular shapes of roughness with various aspect ratios.

Different shapes of laboratory roughness elements like cylinders, cubes, spheres, and rods are primarily classified in two groups (Raupach et al., 1991); two- and three-dimensional roughness elements. This study deals largely with the two-dimensional rod roughness geometry.

Two-dimensional rod roughness

For transverse square 2–D rod roughness (see Figure 1.2), the relevant length-scale is the height of the bar, r. Other relevant length-scale is the roughness spacing, w. Perry et al. (1969) called roughness with $w/r > 1$ the "k–type roughness" since roughness effects showed clear dependency on their roughness height, k. They also showed that the k–type scaling is not obeyed when roughness constitutes narrow cavities (i.e. $w/r \leq 1$). In fact, the flow quantities scaled themselves with the pipe diameter, d. Since then, such a roughness has come to be known as the "d–type roughness".

Figure 1.3 provides a phenomenological schematic of the salient features of the interaction of rod-type roughness and the turbulent boundary layer. The dominant features of the interaction are flow separation and reattachment. These regions of separated flow give rise to a *momentum sink*, which results in the *form drag* of the element.

If the rod spacing is large enough, the boundary layer reattaches to the wall at some point between the rods. The quantitative aspects of these separations and reattachments are highly dependent upon the rod-roughness geometry and attributes of the overlaying turbulent boundary layer. Thereupon, the flow over rod roughness can be divided into three regimes (Hodge et al., 1989):

1. Reattached flow – the separated region behind the rod reattaches to the

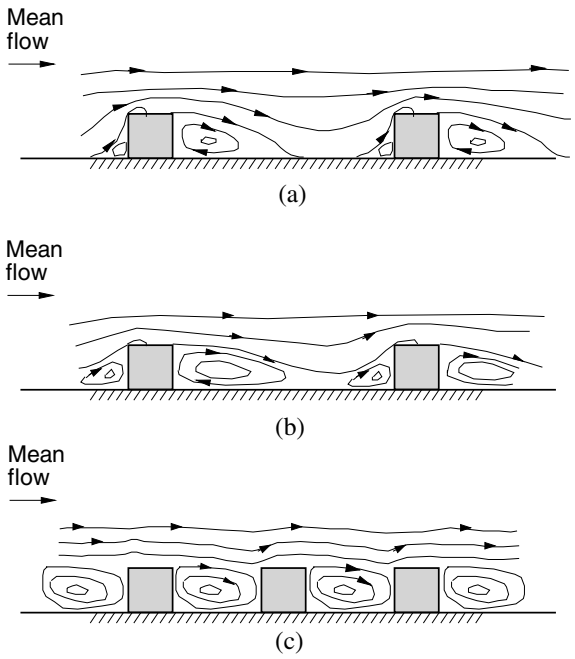

Figure 1.3: Regimes of the mean flow over rod roughness; (a) reattached flow, (b) unreattached flow, (c) skimming flow. The roughness configuration in (a) and (b) is k-type whereas in (c) is d-type.

smooth surface between the rods (bottom wall); viscous skin friction is a significant factor.

2. Unreattached flow – the separated regions behind and in front of the rods merge; viscous skin friction is relatively unimportant.

3. Skimming flow – the region between the rods is completely filled with a recirculating flow; the surface appears semi smooth.

An important point about the relative size of the roughness elements should be noted here. Implicit in the analysis of turbulent flows over wall-mounted roughness elements is the premise that the roughness height should be very small compared to the bulk flow dimension so that roughness elements do not directly affect the outer layer. According to the recent review of Jiménez (2004), the roughness height should not exceed 2.5% of the characteristic length of the overlaying boundary layer. In turbulent flows over rough walls with relative roughness larger than 0.025, it is likely that direct roughness effects are felt across the boundary layer thickness. Turbulent

flows of such will therefore be better described as flows over surface mounted *bluff bodies* rather than roughness elements.

1.3 Incentives

The interaction of classified laboratory roughness elements and the overlaying boundary layer has long been investigated. A thorough review of mainly experimental studies on rod roughness showed that notwithstanding the broad range of research work, there is a lack of consensus on several issues. Issues on which harmony exists is mainly the mean velocity, for which a great deal of data is available and well documented. However, the effects of roughness on turbulence is mainly controversial.

The fundamental idea of the current research program was initiated from the extensive measurements of different types of roughness by Krogstad & Antonia (1999) and Antonia & Krogstad (2001). Assisted by the availability of supercomputers to calculate turbulent flows, a research program for a comparative study of rough-wall turbulence was established.

This was implied through performing measurements in the lab and numerical simulations on the supercomputers for a turbulent flow in a channel with both walls roughened by identical transverse rods. Rod roughness, as it mentioned earlier, provides a considerably rough boundary for the overlaying turbulent flow. Roughness effects of this type have been observed to be substantial. The motivation for this project came from the idea of performing measurements and numerical simulations for the similar roughness geometry emerged in an internal flow, i.e. the channel flow.

1.4 Objectives

The present investigation aims to perform direct numerical simulation (DNS) of the turbulent flow in a rod-roughened channel with roughness elements height equal to only 3.4% of the channel half-height. An extensive database is obtained by calculating all sorts of statistical correlations between the frequent flow quantities. The obtained results are compared to those obtained from the DNS of a turbulent flow at virtually the same Reynolds number in an identical channel with smooth walls.

Comparison with experiments constitutes another objective of this work. Whereas DNS is capable of providing detailed information about the flow field specially in the rough-wall proximity, the experiments are capable of providing data for a broad range of Reynolds number. Doing the DNS and experiments simultaneously provides comprehensive database which gives clues towards a better understanding of turbulent flows in a channel with roughened walls. The significance here is that

no compromise has been made on the shape and size of the roughness elements in both experiments and numerical simulations. The experimental part of this work has been presented by Bakken (2004).

In chapter 2, a thorough review on rod-roughness turbulence research is presented. Mathematical formulation, numerical scheme and the simulation setup are discussed in Chapter 3. A summary of articles resulted from this investigation is presented in Chapter 4.

Chapter 2

Rough-wall Turbulence

The wonderful thing about scaling is that
you can get everything right
without understanding anything.
Robert H. Kraichnan[1]

During the last few decades, a considerable amount of data on rough-wall turbulence has been generated. This chapter presents a brief review on part of this data concerning the k–type rod-roughness. Several issues on the mean and turbulence fields are addressed.

2.1 Mean velocity scaling

Wall turbulence is a multi-scale problem. In 1930, Theodore von Kàrmàn, introduced the similarity assumption that the averaged velocity profile in the outer layer is independent of the molecular viscosity, but its deviation from the center-line velocity, U_{CL}, must be only dependent on the pipe diameter and indeed, the friction at the wall. He deduced the well known *velocity defect law* for the outer layer region of the pipe flow as

$$\frac{\langle U_{CL}\rangle - \langle U_s\rangle}{u_\tau} = F\left(Y\right), \tag{2.1}$$

where $Y = y/\delta$ is a non-dimensional variable. Subscript "s" denotes the quantities associated with the smooth wall and $\langle\ \ \rangle$ is used for averaged quantities. The quantity,

$$u_\tau = \left(\frac{\tau_w}{\rho}\right)^{1/2}, \tag{2.2}$$

[1]As cited by Kadanoff (1990).

is termed the *friction velocity* only because of its dimensions. δ is the thickness of the shear layer equivalent to the pipe radius in pipe flow, the channel half-height in channel flow and the boundary layer thickness in turbulent boundary layer flow. τ_w is the given friction stress at the wall. Using u_τ and δ for normalizing the velocities and lengths is called *outer scaling*.

In the subsequent discussion to the lecture of Theodore von Kàrmàn at the Third International Congress for Applied Mechanics in Stockholm, 25 August 1930, where he presented his universal logarithmic law for boundary layer flows at high Reynolds numbers, Ludwig Prandtl presented his *law of the wall* as he said (Barenblatt, 1999):

> "I want to point out a seeming contradiction concerning both representations of the velocity distribution by Nikuradse in connection with Kàrmàn's new formulas and my earlier formulation using the dimensionless distance from the wall. Kàrmàn formulas use viscosity in the boundary condition only. The velocity distribution should be calculated without viscosity. However, the dimensionless distance from the wall ($y^+ = yu_\tau/\nu$) does contain the viscosity. According to my opinion, the explanation is that the Kàrmàn representation should be considered as exact for very large Reynolds numbers, whereas the representation via the dimensionless distance from the wall applies essentially to the wall layer and streaks where the viscosity and turbulence are acting together."

By dimensional analysis this is equivalent to

$$\frac{d\langle U\rangle}{dy} = f(\eta). \tag{2.3}$$

Here, $\eta = y/\delta_v$ is the non-dimensional variable in which the *viscous length scale*, δ_v, is a length scale for the small eddies whose definition is based on the kinematic viscosity,

$$\delta_v = \frac{\nu}{u_\tau}. \tag{2.4}$$

Using the "wall units" (u_τ, δ_v) in normalizing velocities and lengths is called *inner scaling*. Quantities normalized in this way are identified by a $^+$ superscript.

By postulating that the turbulent fluctuations in the neighborhood of any two points are similar, Kàrmàn derived a velocity profile expressed by a logarithmic function of the distance from the wall. Prandtl (1933) also showed that the assumption of the mixing length proportional to the distance from the wall yields the logarithmic velocity profile. Independently, in 1937, C. B. Millikan showed that the logarithmic velocity profile is a direct outcome of the existence of a region of overlap, without need for any specific assumption on similarity or mixing length. The classical *logarithmic law* in the overlap region ($y^+ > 30$) is

$$\left\langle U^+ \right\rangle = \frac{1}{\kappa}\ln y^+ + B_s. \tag{2.5}$$

Over the full range of Reynolds numbers for internal and external turbulent flows, the dimensionless von Kàrmàn constant, κ, is probably universal and equal to approximately, 0.41. The constant B_s, however, has to be determined independently. It controls the friction coefficient and is about 5.5 for channel flows.

Today, we know that the first important characteristic of wall shear flows is the presence of a strong mean velocity gradient at the wall, which provides a continuous source of kinetic energy for the turbulence to be self-sustained. Wall flows are also intrinsically in-homogeneous. The distance to the wall, in particular, imposes a length scale which governs the size of turbulent motions (*eddies*) from a fraction of the channel half-height to virtually zero at the wall in the infinite Reynolds number limit. This important restriction on the size of turbulent eddies can be formulated by the inequality

$$\delta_v \ll y \ll \delta. \tag{2.6}$$

The classical approximation to the velocity scale is that the friction velocity, u_τ, acts as a global velocity scale. The reason can be found through implication of the thin-layer approximation to the momentum equations. Doing so, it can be observed that the order of magnitude of the turbulent shear stresses is u_τ^2 across the shear layer. These approximations imply that all the near-wall activities should collapse in these wall units (u_τ,δ_v). In fact, it is likely to suppose that many properties of smooth pipe and channel flows depend largely on the nature and properties of the near-wall activities and very little on the flow outside the wall-region.

The region $y^+ \leq 100$ is usually considered as the *wall region*; this includes the *viscous sublayer* ($y^+ < 5$), the *buffer region* ($5 < y^+ < 30$), and at least, part of the logarithmic region. The rest of the shear layer is commonly referred to as the *outer region*. In pipe and channel flows this can include the core region as well.

The logarithmic law, i.e. resulted solely by intuitive reasoning, is likely to be valid for turbulent flows over rough walls too. There is no reason why the roughness height, r, should not be the relevant length scale, if the Reynolds number is sufficiently high and roughness height, r, is very large compared with the viscous length scale, δ_v, i.e.,

$$\delta_v \ll r \ll y \ll \delta. \tag{2.7}$$

Thereupon, Equation (2.3) can be rewritten as

$$\frac{d\langle U_r \rangle}{dy} = f_r\left(\frac{y}{r}\right) \tag{2.8}$$

where f_r is a universal non-dimensional function for a given roughness geometry. Subscript "r" denotes the quantities associated with the rough wall.

For $y \gg r$ it can be supposed that the turbulence is again determined by local processes, independent of r (the Reynolds number similarity) which implies that f_r

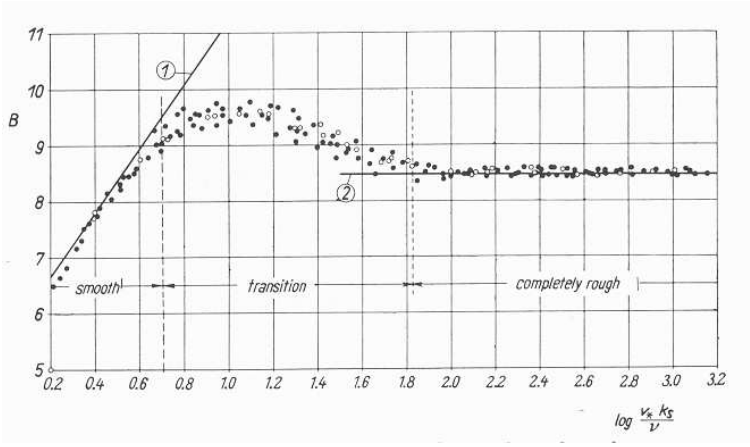

Figure 2.1: Constant B_{sand} in terms of roughness Reynolds number for Nikuradse's sand roughness experiments. Figure from Schlichting (1968).

tends asymptotically to the constant $1/\kappa$. Then Equation (2.8) integrates to the logarithmic law

$$\left\langle U_r^+ \right\rangle = \frac{1}{\kappa} \ln\left(\frac{y}{r}\right) + B_r. \tag{2.9}$$

Writing this equation for $y = \delta$, and forming the $\left\langle U_{rCL}^+ \right\rangle - \left\langle U_r^+ \right\rangle$, we obtain the velocity-defect equation for the rough wall

$$\left\langle U_{rCL}^+ \right\rangle - \left\langle U_r^+ \right\rangle = -\frac{1}{\kappa} \ln\left(\frac{y}{\delta}\right) \tag{2.10}$$

which is independent of r, implying the similarity in the core region.

The constant B_r in Equation (2.9) is generally a function of the roughness Reynolds number, ru_τ/ν, and the roughness density. We use subscript $_{sand}$ instead of r, particularly for the Nikuradse's data. The values of B_{sand} are shown in Figure 2.1. For the fully rough regime over sand grain roughness ($k_s^+ > 70$), $B_{sand} = 8.5$.

It is convenient to rewrite the Equation (2.9) in the form

$$\left\langle U_r^+ \right\rangle = \frac{1}{\kappa} \ln y^+ + B_s - \Delta U^+ \tag{2.11}$$

in which

$$\Delta U^+ = \left\langle U_s^+ \right\rangle - \left\langle U_r^+ \right\rangle = \frac{1}{\kappa} \ln r^+ + B_s - B_r, \tag{2.12}$$

is called the *roughness function*. The sole effect of roughness is neatly characterized by 2.12 as a downward shift in the velocity profile in the logarithmic law region

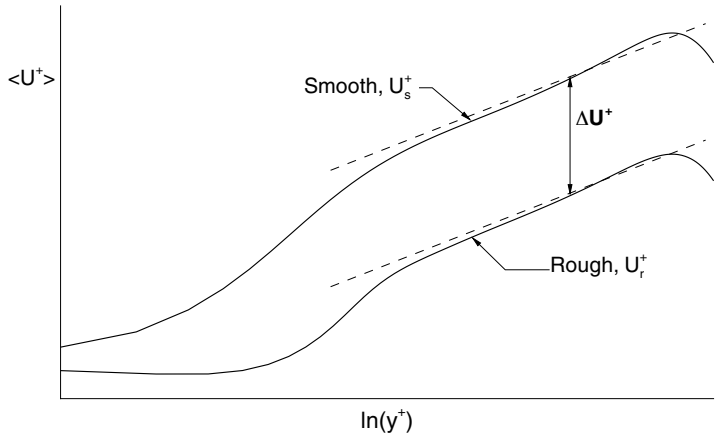

Figure 2.2: Illustration of roughness function.

(Figure 2.2). The fact that the shifts in the velocity for turbulent flow over rough surfaces are linear in the logarithmic plot can be used to express different roughness geometries in terms of a reference roughness (the concept of equivalent sand-grain roughness). It follows that k_s is an equivalent sand-grain size which produces same amount of downward shift in the log-law as that of arbitrary roughness with height r, or, $\Delta U^+_{sand} = \Delta U^+_r$. From this definition the ratio between the equivalent sand roughness and the actual roughness height can be obtained as

$$\frac{k_s}{r} = \frac{\exp[\kappa(3.0 + \Delta U_r^+)]}{r^+}. \tag{2.13}$$

Betterman (1965), using two-dimensional rod roughness with varying spacing, was able to correlate his measurements in terms of Equation (2.12), with the constant $\Delta B = B_s - B_r$ as function of spacing (see Figure 2.3). Betterman observed that for a certain spacing of the rods, the measured value of ΔU^+ was maximum. Betterman found that for the pitch-to-height ratio $\lambda = p/r$ in the range $1 \leq \lambda \leq 5$, the variation of ΔU^+ with roughness could be specified by

$$\Delta U^+ = 2.43 \ln r^+ + 17.35(0.706 \ln \lambda - 1), \tag{2.14}$$

which is plotted in Figure 2.3. This equation shows that ΔU^+ varies logarithmically with λ. It can be seen from the Figure 2.3 that the roughness function is maximized for values of λ between 4 and 8. The extension Betterman's equation for $\lambda > 5$ was accomplished by Dvorak (1969) who proposed

$$\Delta U^+ = 2.43 \ln r^+ - 5.95(0.706 \ln \lambda - 1). \tag{2.15}$$

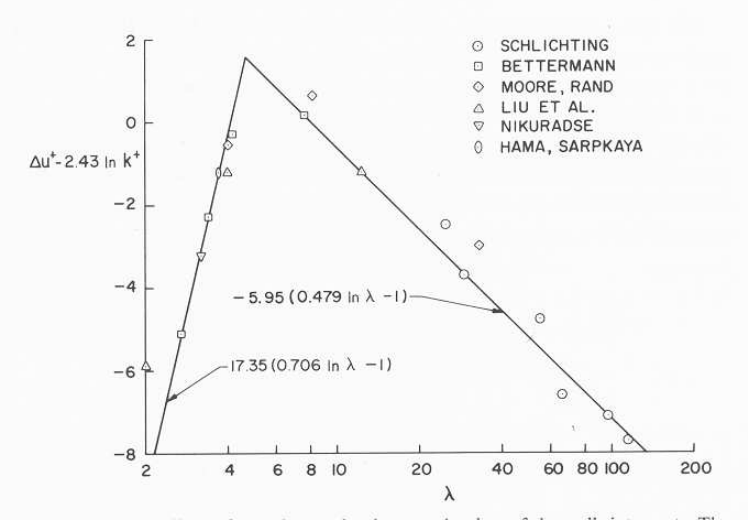

Figure 2.3: The effect of roughness density on the law-of-the-wall intercept. The quantity λ is the ratio of the total surface area to the area covered by roughness. Picture from Cebeci & Smith (1974).

It should be noted that Equation (2.15) requires further verification before it can be used with confidence.

2.2 Rough-wall similarity

As stated in Raupach's review of rough-wall turbulent boundary layers (Raupach et al., 1991), the effect of surface roughness is primarily felt in the roughness sublayer. Hence, close to the wall, the smooth- and rough-wall boundary layers have quite different structures and are controlled by quite different length–scales. As the roughness effect is supposed to be confined to the wall region, the mean velocity and turbulent stresses in the outer layer should then be very little affected. This important assumption, is known as *wall similarity hypothesis* (labeled after Perry & Abell (1977)) which is an extension to Townsend's Reynolds number similarity hypothesis (Townsend, 1976). The wall similarity hypothesis found itself to be well supported by various observations. Through the experiments of Grass (1971) and Grass et al. (1993), the investigation of Perry & Abell (1977); Perry et al. (1987), the comprehensive review of Raupach et al. (1991), measurements of Schultz (2000) and Bergstrom et al. (2002) and the particle image velocimetry (PIV) investigations of Nakagawa & Hanratty (2003). This hypothesis has been extensively used by other

researchers to estimate the value of the skin friction coefficient, C_f (Furuya & Fujita (1967), Bandyopadhyay (1987) and Perry et al. (1987)).

However, studies of Krogstad et al. (1992), Krogstad & Antonia (1999), Djenidi et al. (1999) and Smalley et al. (2002) showed that the large-scale organized structures present several structural differences between the smooth- and rough-wall conditions. In fact, it was Townes & Sabersky (1966) who first reported results from their pioneering work in flow visualizations of a d–type rough-wall turbulent boundary layer, that there are indications of possible significant communication, albeit of an intermittent nature, between ejections of fluid from the roughness cavities and the outer region of the boundary layer. On the basis of differences observed between turbulent boundary layers over a smooth surface and a surface roughened by a mesh screen, the wall similarity hypothesis was first questioned by Krogstad et al. (1992). They observed distinct differences in the outer region in turbulent field between smooth- and rough-wall boundary layers. This was in clear contradiction to the wall similarity hypothesis. Townsend (1993), in the support of his hypothesis, stated that

> "... there must be some doubt about the necessity for bursts being set off by conditions in the sublayer since the turbulent motion over rough boundaries [*in the outer layer*], scaled with friction velocity and flow width, is not distinguishable from that over smooth ones."

Krogstad & Antonia (1994) measured the inclination angle of the two-point correlation function of u between two y locations. They obtained 38^o in the rough case and 10^o in the smooth case. Jiménez (2004) argued that this might be a local effect since the measurements were done fairly near the roughness sublayer. Nakagawa & Hanratty (2003) found no change in this quantity in their PIV measurements on wavy surface. Krogstad & Antonia (1994), in particular, stated that there is clearly much more activity associated with the wall-normal velocity fluctuation over the rough surface than that of the smooth surface. The previous observations, *inter alia*, suggest that there may be a fundamental difference in the momentum transport process between rough- and smooth-wall boundary layers, contrary to what it is thought to be.

2.3 Turbulence above the rough wall

Whereas there is considerable consensus among the community that law-of-the-wall holds for the mean velocity profile over all types of rough surfaces, there is no consensus on the effect of roughness on turbulence. In this section some results from various measurements of turbulence on two-dimensional laboratory roughness are presented in order to show salient features of the arguments.

2.3.1 Second-order moments of velocity fluctuations

Reynolds normal stresses are the primary indicators of characteristics of turbulence. (Hereinafter, u, v, w are the fluctuating components of the instantaneous velocity in the streamwise, wall-normal and spanwise directions, respectively.) A consequence of rough-wall similarity hypothesis is that, provided that Reynolds number is sufficiently high, profiles of the Reynolds stresses should all collapse regardless of surface roughness. Raupach (1981) tested this directly in zero pressure-gradient boundary layer over five fully rough surfaces of different densities and found out that the normalized profiles of Reynolds stresses collapsed to common curves except in the roughness sublayer.

Krogstad & Antonia (1999) compared some earlier measurements carried out for two different types of roughness (mesh screen and circular rods). Despite the difference in geometries and characteristic lengths, all roughness geometries virtually revealed the same dynamical effect (i.e. ΔU^+). Very close to the wall, $\langle u^2 \rangle$-profiles for different roughness shapes showed very good collapse, while considerably large scatter was found in $\langle v^2 \rangle$. Perry et al. (1987) argued that this type of scatter is may be due to the uncertainty of X-wire measurements near the wall. Krogstad et al. (1992) questioned the validity of this claim and noted that possible measurement errors may only explain the differences observed very close to the wall, while such differences are found everywhere; even in the outer layer where the similarity hypothesis predicts the flow to be identical to the flow over a smooth surface.

Previous observations brought Krogstad & Antonia (1999) to an important conclusion that although very different surface geometries may produce the same effect on the mean velocity profile, their generated turbulence fields may be substantially different. Raupach's results from measurements on vertical cylinders as roughness elements (Raupach, 1981) was not supporting this.

Significant wall effects were observed for the k–type rod roughness (Krogstad & Antonia, 1999; Antonia & Krogstad, 2001). The normal stress, $\langle u^2 \rangle$, indicated considerable reductions in the inner layer, but there were also discernible differences in the outer layer. Larger differences, however, were found in the wall-normal stress, $\langle v^2 \rangle$. This observation implied reduced damping effect of the rough wall in suppressing the wall-normal Reynolds stress to zero. In other words, in the roughness sublayer, wall-normal motions were stimulated and the information about the nature of the surface protruded further out, which caused a higher magnitude of normal and shear stresses in the outer layer.

2.3.2 Ratios and anisotropy of Reynolds stresses

While knowledge of a local value for u_τ is important in understanding of the turbulent structure near the wall surface, Reynolds stresses can be compared between

different boundary layers without knowing the magnitude of u_τ. Ratios such as $\langle v^2 \rangle / \langle u^2 \rangle$, $\langle v^2 \rangle / \langle w^2 \rangle$ or $\langle uv \rangle / \langle v^2 \rangle$ provide a rough indication of the departure of the Reynolds stresses from isotropy. Shafi & Antonia (1995) and Antonia & Krogstad (2001) observed that the anisotropy, was reduced over a rough wall. This was more prominent for k–type roughness (Smalley et al. (2002)). Results apparently reflected the ability of the roughness to distribute the turbulent energy more evenly among the three velocity fluctuations. According to the apparent differences exist in AIM of different roughness elements, Smalley et al. (2002) proposed the idea that each rough wall can be characterized by its own AIM signature.

2.3.3 Third-order moments of velocity fluctuations

Velocity triple products are expected to be a more sensitive indicator of the effect of surface condition than second-order moments. Despite the numerous investigations on smooth and rough walls, the behavior of third–order moments of the velocity fluctuations did not seem to make a general consensus (Keirsbulck et al., 2001). Moreover, the measurements of these statistical quantities on rough-wall remained scarce, unlike higher even moments which contain valuable statistical information relating to the flux of the stress that is directly attributable to coherent structures.

Andreopoulos & Bradshaw (1981) noted that triple products were spectacularly altered for a distance up to 10 roughness heights above a surface covered with floor-sanding paper. Bandyopadhyay & Watson (1988) reported that instantaneous motions involved in the shear stress flux near the wall in smooth and transversely grooved surfaces are opposite in sign to those over a three-dimensional roughness. Antonia & Krogstad (2001) reported major differences in distributions of $\langle u^2 v \rangle$ and $\langle u^3 \rangle$ between the rod and mesh screen types of roughness. Both triple products change sign above the rod-roughened wall. There is pronounced transport of $\langle u^2 \rangle$ and $\langle v^2 \rangle$ towards the wall over the rods, contrary to what happens over the mesh-screen roughness where the transport is away from the wall.

2.4 The structure of rough-wall turbulence

In turbulent boundary layer, kinetic energy from the free-stream flow is converted into turbulent fluctuations and then dissipated into internal energy by viscous action. It is known that there are coherent motions that are actually responsible for the maintenance of turbulence in a boundary layer. Robinson (1991) proposed the following definition for the *coherent motion* in turbulence:

> Coherent motion is a three-dimensional region of the flow over which at least one fundamental flow variable exhibits significant correlation with

> itself or with another variable over a range of space and/or time that is significantly larger than the smallest local scales of the flow.

The term coherent motion has been used interchangeably with *turbulent structure* in the literature. Here, a short review of studies on rough-wall turbulent structures is presented.

2.4.1 Quadrant analysis

For rough walls, quadrant analysis was first employed to study the coherent structures by Grass (1971). Even though the near-wall streaks were considerably affected by the roughness elements, Grass observed, for gravel type surface roughness, that the ejections and sweeps were similar to those previously identified over smooth walls. Lumps of low-momentum fluid were ejected from the boundary to the distances remote from the wall. Similarly, he observed that maximum local longitudinal velocities correlate directly with packed regions of negative vertical velocity. For the rough case he stated that phases of fluid inrush towards the boundary is concentrated closer to the boundary. Raupach (1981) also found that the sweep events are very important close to the wall and depend on the roughness density.

Krogstad et al. (1992) showed that the normalized contributions to the Reynolds stress for the Q_2 and Q_4 quadrants are very intense on rough walls and their occurrence frequency is twice as high as on smooth walls. Nakagawa et al. (2003) and Nakagawa & Hanratty (2003) performed Laser Doppler Velocimetry (LDV) for turbulent flows over a flat surface and one with sinusoidal waves of small wavelength at all three different regimes (hydraulically smooth, transitionally, and fully rough). Comparisons with data from a previous direct numerical simulation (Cherukat et al., 1998) of turbulent flow in the same geometry were also provided. The quadrant analysis showed much smaller contributions from the sweeps and much larger contributions from ejections in turbulent flow over wavy wall at fully rough regime. This observation was consistent with those from the DNS results that large scale ejections of low momentum fluid propagate from the trough region of the waves. However, the structure of large-scales was claimed to be similar to those over the smooth wall notwithstanding of large difference in the ratio of the contributions of the second and fourth quadrants (Q_2/Q_4) throughout the boundary layer. The ratio Q_2/Q_4 was significantly larger over rough surface than that over the smooth one.

2.4.2 Small-scale turbulence

Following the observation of large-scale turbulence on rough walls, one would expect that the small-scale turbulence structure to be closer to isotropy in the rough wall layer.

Shafi & Antonia (1997) measured same quantities in similar flow using a four-hot-wire vorticity probe in which the effect of spatial resolution of the probe was corrected. They observed that the vorticity variances were slightly larger than those over a smooth wall in the outer layer; suggesting structural differences between the two flows. They also measured the normalized magnitudes of the velocity derivative variances, $\left\langle (\partial u_i/\partial x_j)^2 \right\rangle^{1/2}$, and observed that over most of the outer layer, they differ significantly from those over a smooth wall layer such that the flow over the rough wall was much more isotropic than that over the smooth wall.

Ratios of variances of velocity derivative and vorticity are all equal to 1 for isotropic turbulence. Shafi & Antonia (1997) measured these ratios for a boundary layer flow over a mesh roughness and observed that all the ratios were approximately equal to 1 over a significant portion of the layer.

2.5 Boundary layer vs. channel flow

Whereas the structure of turbulence over rough surfaces have been extensively investigated by means of various experiments performed on the rough-wall turbulent boundary layers (§2.4), turbulent flows in channels with rough walls have not been investigated alike (e.g. Mazouz et al. (1994, 1998) and Smalley et al. (2002)).

The geometrical difference between the channel and the boundary layer flow are of prime importance. It is generally accepted that a high degree of similarity exists between the internal flows (pipe and channel flows) concerning at least the near-wall behavior, whereas the zero-pressure-gradient boundary layer flow stands out because of its spatially developing character. A short but very useful study of similarities and differences of turbulent boundary-layer, pipe and channel flow is presented by Nieuwstadt & Bradshaw (1997). The turbulent/non-turbulent interface, an important feature of the boundary layer, is absent in the channel flow. Instead, there are back-to-back shear layers near the channel centerline. The shear stress gradient is small in the inner region of a constant pressure-gradient boundary layer, but not in a fully developed channel flow where it is balanced by the streamwise mean pressure gradient (Antonia et al., 1992). There is also possibility that inner region structures from the opposite walls (in case of channel flow) do in fact interact. This possibility is greater at low Reynolds numbers. Because of this so-called "geometry effect" (Wei & Willmarth, 1989), one might expect differences between the outer regions of a boundary layer and a duct. Using quadrant analysis, Teitel & Antonia (1990) showed that the extent of penetration of one shear layer into the opposite side is in fact greater than what it was proposed by Dean & Bradshaw (1976), who claimed that the interaction is insignificant.

Jiménez (2004) suggested that in the boundary layers, "there are vertical struc-

tures that span the whole boundary layer thickness and feel the outer-edge conditions". The important difference between the channel and boundary layer flows is that in the former, the excessive energy is transported by turbulent diffusion to the core region where it compensates the dissipation, whereas in the latter, the extra energy is used to sustain the thickening of the layer. How surface roughness alters this scenario in both flows, is still unknown.

2.6 Numerical simulation of rough-wall turbulence

Since 1980, because of the significant improvements made in modern super-computing technology, direct numerical simulation (DNS) has become an effective tool in providing invaluable insights into the nature of turbulence (Kim et al., 1987). Nonetheless, very few DNS of rough-wall boundary layer flows have been reported. Angelis et al. (1997), Cherukat et al. (1998), Henn & Sykes (1999) and Sullivan et al. (2000), performed numerical simulations of turbulent flows over wavy walls. The amplitudes, a, of the waves were however, too large to be considered as surface roughness. Nakayama & Sakio (2002) performed a DNS of flows over rough wavy boundaries in view of obtaining a model for subgrid scale modelling. The relative roughness, a/δ for their case was 0.1. Miyake et al. (2000) performed a DNS of turbulent flow at $Re_\tau = 400$ in a channel where one wall was roughened by modelled cone-shape roughness elements. The average roughness height to channel half height ratio was about 0.06. Roughness Reynolds number was $r^+ = 25$ which created a roughness function $\Delta U^+ = 7.5$. Miyake et al. (2001) performed the similar DNS in a turbulent channel flow with rod roughness operating at $Re_\tau = 150$. For this case the ratio r/h was the large value of 0.13. Leonardi et al. (2003) also carried out a DNS for a fully developed channel flow with a rod-roughened bottom wall and smooth upper wall. The height of the square bars was about 10% of the channel height. A wide range of pitch-to-height ratio (λ) has been studied. They partly reported their results in Smalley et al. (2002) for two values of $\lambda = 2$ and 5. In the near-wall region, the DNS data highlighted the dramatic variation in the AIM signature over one roughness wavelength, reflecting the significant changes in turbulence state which may occur between consecutive roughness elements. DNS of one-sided rod-roughened channel flow has also been performed by Ikeda & Durbin (2002) and Nagano et al. (2003), whereas results of a LES were presented by Cui et al. (2003). A common feature of all these earlier computer simulations is that only one channel wall was roughened whereas the other wall remained smooth. The height of roughness elements was typically in between 5% and 10% of the channel height.

Results from the direct numerical simulation of turbulent incompressible plane-channel flow between a smooth wall and one covered with regular three-dimensional

"egg carton"-shaped roughness has been recently published by Bhaganagar et al. (2004). They compared results from the smooth- and rough-wall sides of the channel for three different roughness heights of $r^+ = 5.4$, 10.8, and 21.6 for Re_τ of 400. They focused on the interaction between the near-wall and outer-layer regions, in particular the extent to which the near-wall behavior influences the flow further away from the surface. They observed that roughness tends to increase the intensity of the velocity and vorticity fluctuations in the inner layer. In the outer layer, although the roughness altered the velocity fluctuations, the vorticity fluctuations were relatively unaffected. The higher-order moments and the energy budgets demonstrated significant differences between the smooth-wall and rough-wall sides in the processes associated with the wall-normal fluxes of the Reynolds shear stresses and turbulence kinetic energy. They found that the strength of the inner/outer-layer interactions are greatly affected by the size of the roughness elements.

Flores & Jiménez (2004) proposed a different approach towards the DNS of rough-wall channel flow. The idea was to simulate the effect of roughness on the flow without having to deal with the details of the flow around them. The no-slip and impermeability boundary conditions were replaced by prescribed zero-mean-value perturbed velocities with characteristic intensity and wavelengths. The first consequence of these disturbances was the generation of non-steady separation bubbles at the wall, the averaged height of which was taken as the roughness height. For all cases presented ($24 < k_s^+ < 207$), the intensities collapsed in the outer regions, indicating that the classical similarity holds disagreeing with Krogstad et al. (1992). They also observed that away from the wall, the flow recovers the organization typical of flows over smooth walls.

Chapter 3

Numerical Simulation

The set of differential equations governing incompressible fluid flow and the numerical scheme for solving these equations are discussed in this chapter. Detailed information about the numerical simulation set up is also presented.

3.1 Governing equations

The sole dynamics of the turbulent flow field, i.e. the spatial and temporal evolutions of a fluid differential-element, is completely described by mass continuity and the Navier-Stokes equations. These equations for an isothermal, incompressible fluid are

Continuity

$$\frac{\partial U_j}{\partial x_j} = 0 \tag{3.1}$$

Navier-Stokes

$$\frac{\partial U_i}{\partial t} + \frac{\partial U_i U_j}{\partial x_j} = -\frac{1}{\rho}\frac{\partial P}{\partial x_i} + \nu\frac{\partial T_{ij}}{\partial x_j} \tag{3.2}$$

where U_i stands for the velocity in the i-th direction and P for the modified pressure. T_{ij} is the deviatoric stress tensor given by

$$T_{ij} = \left(\frac{\partial U_i}{\partial x_j} + \frac{\partial U_j}{\partial x_j}\right), \tag{3.3}$$

and ν is the kinematic viscosity defined by $\nu = \mu/\rho$, where μ, is the dynamical viscosity of the fluid and, ρ, is the density. A summation is understood for repeated indices. Indices are 1,2,3 respectively for the streamwise, vertical and spanwise directions. The frame of reference is an inertial Cartesian (x, y, z) coordinates. Here, $(x, y, z) \equiv (1, 2, 3)$.

Each of the quantities in the above equations are instantaneous and generally, random functions of space and time. In direct numerical simulation (DNS), the governing equations 3.1 and 3.2 are solved numerically without any further assumptions, to the finest spatial and temporal scales possible. If possible, a conventional spatial and temporal averaging will then be performed in order to obtain statistically steady state averaged quantities and the associated unsteady instantaneous counterparts. For each flow quantity Φ,

$$\Phi = \langle \Phi \rangle + \phi$$

where $\langle\rangle$ is used in order to denote the averaged part and ϕ is the associated fluctuating part. This is the treatment first proposed by Osborne Reynolds in 1895. Thereupon, the *Reynolds-Averaged Navier-Stokes* (RANS) equations can be derived as

$$\frac{\partial \langle U_i \rangle}{\partial t} + \frac{\partial \langle U_i U_j \rangle}{\partial x_j} = -\frac{1}{\rho}\frac{\partial \langle P \rangle}{\partial x_i} + \nu \frac{\partial \langle T_{ij} \rangle}{\partial x_j} - \frac{\partial \langle u_i u_j \rangle}{\partial x_j}. \tag{3.4}$$

The quantity $-\rho \langle u_i u_j \rangle$ has same dimension as that of stress and is a second order symmetric tensor. Therefore, it is called the Reynolds stress tensor. However, for the sake of simplicity, $\tau_{ij} \equiv \langle u_i u_j \rangle$ is conveniently referred as Reynolds stress tensor.

For the fully developed turbulent flow inside a plane channel with smooth walls, the momentum Equation (3.4) can be simplified and directly integrated to obtain the total shear stress ($\tau_{total} \equiv \mu \frac{d\langle U \rangle}{dy} - \rho \langle uv \rangle$) variation across the channel height as

$$\tau_{total} = \tau_w \left(1 - \frac{y}{h}\right). \tag{3.5}$$

Therefore, for every given wall shear stress, τ_w, the total shear stress has a linear profile independent of fluid properties (ρ and μ) and regardless of the state of fluid motion. The friction velocity based on the pressure-gradient is

$$u_\tau \equiv \sqrt{\frac{-h}{\rho}\frac{d \langle P \rangle}{dx}}, \tag{3.6}$$

where h is the channel half-height.

In flows over rough surfaces, the roughness elements distort the streamwise mean flow in the near-wall region such that the mean wall-normal velocity component, $\langle V \rangle$, obtains considerable magnitudes at the proximity of the rough wall. The streamwise momentum equation for the rough-wall channel flow can then be written as

$$\frac{\partial}{\partial x}\left(\nu \frac{\partial \langle U \rangle}{\partial x} - \left\langle u^2 \right\rangle - \langle U \rangle^2\right) + \frac{\partial}{\partial y}\left(\nu \frac{\partial \langle U \rangle}{\partial y} - \langle uv \rangle - \langle U \rangle \langle V \rangle\right) = \frac{1}{\rho}\frac{\partial \langle P \rangle}{\partial x}. \tag{3.7}$$

In this case, when all the streamwise variations are negligible compared to their wall-normal variations (like at distances far enough from the wall), the total shear stress is obtained from

$$\tau_{total} = \mu \frac{\partial \langle U \rangle}{\partial y} - \rho \langle uv \rangle - \rho \langle U \rangle \langle V \rangle . \tag{3.8}$$

There is a contribution of mean momentum transport $-\rho\langle U\rangle\langle V\rangle$ to the shear stress. This contribution is absent in case of a smooth channel. This roughness-induced correlation has a direct dynamical effect in the immediate vicinity of the roughness elements and causes the variation of the total shear stress to deviate from the linear profile 3.5. The range of this deviation from linearity indicates the zone of influence of the roughness elements in the channel.

A valuable scalar quantity is the *turbulent kinetic energy*, k, which is defined to be the half trace of $\langle u_i u_j \rangle$,

$$k \equiv \frac{1}{2} \langle u_\ell u_\ell \rangle . \tag{3.9}$$

The significance of k is that it reveals information from the large eddies. The quantity $k^{1/2}$ is frequently used in turbulence modelling as a velocity scale for the large-scale turbulence.

The transport equation for the Reynolds stresses is

$$\begin{aligned}
\tfrac{\partial \langle u_i u_j \rangle}{\partial t} = \; & - \langle U_\ell \rangle \tfrac{\partial \langle u_i u_j \rangle}{\partial x_\ell} && \text{advection rate} \\
& - \langle u_i u_\ell \rangle \tfrac{\partial \langle U_j \rangle}{\partial x_\ell} - \langle u_j u_\ell \rangle \tfrac{\partial \langle U_i \rangle}{\partial x_\ell} && \text{production rate} \\
& - \tfrac{\partial \langle u_i u_j u_\ell \rangle}{\partial x_\ell} && \text{turbulent transport rate} \\
& - \tfrac{1}{\rho} \left\langle u_i \tfrac{\partial p}{\partial x_j} + u_j \tfrac{\partial p}{\partial x_i} \right\rangle && \text{velocity–pressure– gradient term} \\
& + \nu \nabla^2 \langle u_i u_j \rangle && \text{viscous diffusion rate} \\
& - 2\nu \left\langle \tfrac{\partial u_i}{\partial x_\ell} \tfrac{\partial u_j}{\partial x_\ell} \right\rangle . && \text{dissipation rate}
\end{aligned} \tag{3.10}$$

All of the various terms appear in Equation (3.10) can be calculated using the fully resolved three-dimensional flow fields produced by DNS. Applying one contraction on the Equation (3.10) yields the transport equation for the turbulent kinetic energy (TKE).

3.2 Numerical method

The non-dimensional governing equations are solved using an explicit version of the fractional-step method proposed by Chorin (1967) on a staggered Cartesian nonuniform grid in which the pressure, P, is defined at the center of each grid cell and the components of the velocity vector $\mathbf{U}$ at the cell interfaces. Velocity components and their derivatives, which have to be determined at locations between their corresponding locations, are obtained by linear interpolation and central differences, respectively. As a result, the spatial discretization is of second-order accuracy.

Using a Leapfrog scheme for the explicit time integration of the momentum equation with time-lagged diffusion term Manhart (2004), a second-order accuracy in time is achieved by

$$\mathbf{U}^{n+1} = \mathbf{U}^{n-1} + 2\Delta t \left[N(\mathbf{U}^n) + \frac{1}{Re}\nabla^2 \mathbf{U}^{n-1} - \nabla(\mathbf{P}^{n+1}) \right], \tag{3.11}$$

where $N(\mathbf{U}^n)$ denotes the nonlinear convection terms. The solution at the new time level is obtained, by first taking the known pressure at time level n and solving the explicit step

$$\mathbf{U}^{*} = \mathbf{U}^{n-1} + 2\Delta t \left[N(\mathbf{U}^n) + \frac{1}{Re}\nabla^2 \mathbf{U}^{n-1} - \nabla(\mathbf{P}^{n}) \right], \tag{3.12}$$

where $\mathbf{U}^*$ is an intermediate velocity field, calculated by using the old pressure term in Equation (3.12). The pressure at the new time level $P^{n+1} = P^n + \Delta P^{n+1}$ is determined by the solution of the Poisson equation

$$\nabla^2 \left(\Delta P^{n+1} \right) = \frac{1}{2\Delta t} \nabla \cdot \mathbf{U}^{*}. \tag{3.13}$$

A divergence–free field $\mathbf{U}^{n+1}$ is obtained after a velocity correction

$$\mathbf{U}^{n+1} = \mathbf{U}^{*} - 2\Delta t \nabla \left(\Delta P^{n+1} \right). \tag{3.14}$$

The combination of central interpolation and a Leapfrog time–step is energy conserving for the one–dimensional convection equation. In combination with the diffusion operator, however, the Leapfrog time–step is slightly unstable. Therefore, the diffusive term is taken at the time level $n-1$ in Equation (3.12). Every 41 time steps, an averaging step is performed in order to prevent $2\Delta t$ oscillations inherent in the Leapfrog time advancement.

The Poisson Equation (3.13) is solved by an iterative procedure accelerated by a multigrid cycle. The smoother (single-grid iteration) is based on the velocity-pressure iteration presented by Hirt et al. (1975) with over-relaxation, Γ.

The pressure estimate at time-step $n+1$ is obtained from

$$\Delta P^{i+1} = \Gamma \frac{1}{2\Delta t} \left(\nabla \cdot \mathbf{U}^*\right)^i \left(\frac{1}{1/\Delta x^2 + 1/\Delta y^2 + 1/\Delta z^2}\right). \tag{3.15}$$

Components of velocity at time-step $n+1$ are corrected by

$$U_j^{i+1} = U_j^i + \Delta P^{i+1} \frac{2\Delta t}{\Delta x_j} \tag{3.16}$$

and pressure is accordingly corrected by

$$P^{i+1} = P^i + \Delta P^{i+1}. \tag{3.17}$$

With the over-relaxation Γ, this scheme gives the same convergence properties as a conventional Gauss-Seidel iteration with successive over-relaxation (SOR). The advantage of the present algorithm is the easy treatment of boundaries, at which only velocity boundary conditions have to be specified. This has proven useful in simulating arbitrary geometries with an immersed boundary method in Cartesian grids (Manhart et al., 2001*a*).

A multi-grid algorithm is implemented in order to accelerate the convergence of the iterative solver. For the multi-grid cycle, the so-called "restriction" (fine to course level interpolation) is done for each component of the velocity by averaging over four fine-grid velocities. Coarse-grid pressure is obtained by volume averaging. For the so-called "prolongation" (coarse to fine interpolation), only the pressure on the coarse grid is used. Therefore, the velocity correction step (3.16) make use of only the pressure correction introduced by the coarse grid cycle, i.e.,

$$U_j^{i+1} = U_j^i + \left(P_{coarse}^{i+1} - P_{fine}^i\right) \frac{2\Delta t}{\Delta x_j}. \tag{3.18}$$

The described procedure has also the advantage that during the iterations, full control over the residual divergence of the velocity field is obtained.

3.2.1 Stability

For stable simulations of fluid flows by explicit finite difference schemes, the time step must be smaller than a critical time step. The critical time step, Δt_c, is generally smaller than the minimum value found for pure convection and pure diffusion. For the leapfrog scheme these are

$$\begin{aligned} \Delta t &\leq \tfrac{1}{4\mu} \left[\tfrac{1}{\Delta x^2} + \tfrac{1}{\Delta y^2} + \tfrac{1}{\Delta z^2}\right]^{-1} && \text{pure diffusion} \\ \Delta t &\leq \left[\tfrac{|U|}{\Delta x} + \tfrac{|V|}{\Delta y} + \tfrac{|W|}{\Delta z}\right]^{-1} && \text{pure convection} \end{aligned} \tag{3.19}$$

The critical time step must be smaller than the minimum of two time steps above. An acceptable lower boundary for the critical time step is (Schumann, 1975)

$$\Delta t_c = \left[\frac{|U|}{\Delta x} + \frac{|V|}{\Delta y} + \frac{|W|}{\Delta z} + 4\mu \left(\frac{1}{\Delta x^2} + \frac{1}{\Delta y^2} + \frac{1}{\Delta z^2} \right) \right]^{-1} . \tag{3.20}$$

It is convenient to reduce Δt_c by a factor of 0.5 in order to account for nonlinearities.

3.2.2 The code MGLET

The above described numerical scheme is implemented in the computer code MGLET (multi-grid large eddy turbulence) Manhart (2004) which is used for the present numerical simulations. It was originally developed by Werner (1991) and subsequently improved to include parallelization. The computational grid is divided into an arbitrary number of subgrids that are treated as independent grid blocks in parallel processing. MGLET uses a block-structured paradigm in order to manage multiple grids that arise from the parallelization (Manhart et al., 2001*b*). MGLET has a long tradition in large-eddy simulation (LES) and DNS (Friedrich et al. (2001) and Manhart (2004)). Validation of the simulation code has been performed in the course of various DNS and LES studies of turbulent flow in a smooth channel, separating and reattaching turbulent boundary layer flow (Manhart & Friedrich, 2002).

3.3 Numerical simulation setup

Any DNS approach is constrained by the spatial resolution required to resolve all the scales of fluid motion. This constraint is even more pronounced in a DNS of rough-wall turbulent flows where additional grid points are needed in order to fully resolve the flow field in the vicinity and between the roughness elements. Figure 3.1 shows a sketch of the computational domain. A coordinate system is adopted in which x is aligned with the primary flow direction, y is measured vertically from the bottom wall, and z is parallel to the roughness crests.

Boundary conditions

Periodic boundary conditions are applied in the streamwise direction as well as in the spanwise direction. No-slip and impermeability conditions are imposed on all the solid boundaries. For the computational cells within the rods, the so-called *blanking* technique is used, i.e., velocity components are set to zero whereas the pressure is set to an infinitely large number. Same boundary conditions are used for both the intermediate and divergence free velocity fields.

To drive the turbulent flow in the channel, a fixed negative normalized pressure gradient,

$$d\langle P\rangle/dx = -1, \tag{3.21}$$

is imposed throughout the domain. The fixed pressure difference is explicitly enforced as a body force on the right-hand-side of the Equation (3.2).

Roughness geometry

Transverse square rods of cross section $r \times r$, positioned in a non-staggered arrangement are implemented on both walls. The pitch-to-height ratio, p/r, is 8. The roughness height is only $0.034h$, where h is the channel half-height.The roughness size is fairly close to the maximum roughness size, $0.025h$, proposed by Jiménez (2004) in order to be different from bluff bodies. In this study, the roughness size was dictated from the lab where experiments had to be performed on the already decided geometry.

Operating Reynolds number

Based on Nikuradse's measurements, k_s^+ must be greater than 70, in order that turbulent flow be in a fully rough regime. Data from previous measurements on rod roughness showed the following approximate correlation between the roughness Reynolds number, r^+, and its associated normalized equivalent sand grain roughness height, k_s^+:

$$k_s^+ \approx 5r^+.$$

Having $r/h = 0.034$, gives

$$Re_\tau = \frac{hr^+}{r} \simeq \frac{1 \times \frac{70}{5}}{0.034} \simeq 411$$

as the lower bound for the fully rough regime. Therefore, the friction Reynolds number $Re_\tau = 400$ was selected as the operating Reynolds number for the direct numerical simulations.

Computational box

The length L_x and the width L_z of the computational domain were $6.528\,h$ and πh, respectively, i.e. virtually the same as those in the canonical channel flow simulation of Moser et al. (1999) at $Re_\tau = 395$. This was believed to be sufficiently large such that periodic boundary conditions could be used both in the streamwise and spanwise directions. Owing to the idea that roughness elements shortens the coherence length in the streamwise direction, several test simulations on domain

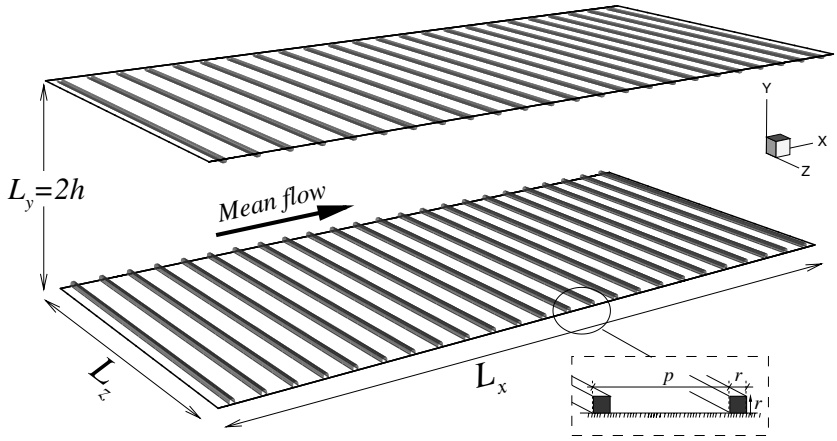

Figure 3.1: Symmetric rod-roughened channel geometry and the configuration of the k–type roughness.

Case	L_x/h	L_z/h	N° of rods
I	$\simeq 3/4\pi$	$3/4\pi$	18×2
II	$\simeq 3/4\pi$	π	18×2
III	$\simeq 2\pi$	π	24×2

Table 3.1: Test cases for the computational domain size study.

boxes with smaller sizes in either or both of the streamwise and spanwise directions were performed. The sufficiency of the computational box size was detected through calculating the two-point correlations in the streamwise and spanwise directions. A summary of the test cases is given in Table 3.3.

The computational box in Case I was too small. Therefore, the channel width, $L_z = \pi$, was used for other two cases. For Case II, the correlation coefficient R_{uu}/u'^2 was sufficiently small at the channel half-length for y^+ up to 40. Towards the channel centerline, however, the correlation factor did not decay to zero, indicating that the channel length was not long enough. Accordingly, the box size was set back to that used by Moser et al. (1999). Calculation of correlation factors for Case III indicated that the computational size was sufficiently large. The computational domain therefore, encompassed 24 square rods on each wall. Alternatively, L_x can be expressed in terms of the roughness characteristics, i.e. $L_x = 192r$.

Case	$N_x \times N_y \times N_z$	Δx^+	Δy_0^{+a}	Δy_{CL}^+	Δz^+	Δt_c^+	$N_P{}^b$	CPU-H
A	$1536 \times 258 \times 258$	1.7	0.85	12.7	4.8	0.036	64	280,000
B	$768 \times 328 \times 192$	3.4	0.85	7.5	6.54	0.04	32	123,000
C	$768 \times 160 \times 160$	3.4	1.7	15.6	7.85	0.06	32	31,000

[a] Within distance $3r$ from each wall [b] Number of processors
[c] CPU hours needed for 30 large eddy turn-over time scales $= h/u_\tau$

Table 3.2: Test cases for the grid independence and feasibility.

Computational grid

The number of grid points resolving each rod face had to be a perfect square in order that the multigrid algorithm could be used for this problem. In the streamwise direction resolving the crest with, e.g., 16 grid points, which gives $\Delta_x^+ = 0.85$, amounted to 3072 uniform grid points. An attempt towards using grid refinement in the streamwise direction not significantly reduce the grid cells in the streamwise direction, unless relatively high stretching/contracting factor is used. A uniform grid is used in the streamwise direction in order to avoid numerical errors which are resulting from intensive grid stretching (a factor larger than approximately 5%),

A uniform distribution of grid points is also used in the spanwise direction. Within the roughness sublayer region (up to $y = 3r$), i.e., $y^+ < 41$, a uniform grid spacing was also used in the wall-normal direction. The mean grid width $\Delta^+ = (\Delta x^+ \Delta y^+ \Delta z^+)^{1/3}$ was therefore kept constant in the near-wall region. Beyond $y = 3r$, Δy^+ was gradually increased towards the center of the channel.

Resolution check and feasibility

The major difficulty in performing this numerical simulation stemmed from the severe restriction on the time-stepping imposed by the diffusion term in the stability criterion for the explicit time-stepping (Equation 3.20) because of a very steep velocity gradient on top of the roughness crest. A number of test cases were created in order to check the grid independence as well as the feasibility of the simulations in terms of the amount of CPU-hours available for this project. Table 3.3 shows various grids which were created and tested. Cases A and B required unaffordable amounts of CPU time. Case C was chosen as the first attempt to this simulation, results of which are presented in this thesis. This was done mainly due to some limitations on the amount of available CPU hours.
The adequacy of the grid resolution in Case D was known to be marginal in the vicinity of the roughness elements, although the imbalance in the budgets of Reynolds

stresses on top of the roughness crest as well as in the cavity region shows acceptable levels (see Article III for details). Since the drag on the roughened walls is larger and the smooth and roughened channels have the same pressure-gradient, the bulk flow rate was reduced for the roughened channel. This reduction is substantial and about 30%. Consequently, the Kolmogrov length, η^+, in the core region of the channel is increased comparing to that of the smooth case. The sufficiency of the grid resolution was studied through the method suggested by Grötzbach (1983) in which $\Delta^+ < \pi\eta^+$. The Kolmogorov length scale was estimated from an earlier channel flow simulation at $Re_\tau = 395$ (see Antonia et al., 1991, Figure 3) to be $\eta^+ \approx 2.5$. At the centerline, the mean grid width was $\Delta_{CL} \simeq 7.5$, therefore the above mentioned criterion is fulfilled.

Turbulent flow initiation

A 3D initial flow field was obtained from a very-large eddy simulation (VLES) of smooth channel flow with $Re_\tau = 400$. The mean velocity, however, was adjusted to the appropriate rough-wall levels. This VLES was based on the most energetic POD modes deduced from an earlier large-eddy simulation. Small-scale modes were randomly imposed to assure some energy in the high wave number part of the spectrum (see Johansson & Andersson, 2004, for details). In the presence of rods the DNS was first advanced forward in time until a realistic turbulent flow field evolved after a time $2\,h/u_\tau$ and a statistically steady state was reached $3\,h/u_\tau$ later.

Evaluation of statistics

The simulation continued for another $20\,h/u_\tau$, during which statistics were computed from individual flow fields equally separated by $0.5\,h/u_\tau$ or 200 viscous time units. In addition to averaging over these 40 nearly independent flow fields, averaging was also performed in the homogeneous spanwise direction. The presence of rods precludes the streamwise direction from being homogeneous. However, since periodically arranged roughness elements induced a streamwise periodicity on the averaged fields, the statistical equivalence of two points (x, y, z) and $(x + np, y, z)$, where p is the pitch and n is an integer, was utilized and unit-wise averaging in the streamwise direction was performed. To further increase the number of statistically independent samples, averaging was also performed between both sides of the channel, thus benefiting from the geometrical symmetry of the rod-roughened channel.

The sampling is done at the staggered mesh locations for different correlations appearing in the Reynolds stress transport equation. The same second order discretization as those employed in the governing equations, were used for all budget

calculations. Boundary conditions at all solid walls were carefully implemented for the various forms of derivatives of the fluctuating velocity field and pressure.

Chapter 4

Summary of Articles

Article I:

Mean flow field and Reynolds stresses

This article mainly discusses issues regarding the effect of the roughness elements on the mean velocity field and the variation of the Reynolds stresses across the channel. The magnitude of the roughness function ΔU^+ was found to be about 7 which suggested that the directly simulated flow field is virtually in the upper end of the transitionally rough regime. It was observed that the two-dimensional rods induced substantial changes in the mean velocity field in certain layers extended about 5 times rod height. Despite the dramatic roughness effects in the roughness sublayer, elongated streamwise streaky structures were observed in a short distance above the plane of roughness crest. Such streaky structures have not been reported in any of the earlier computational studies of rod-roughened channel flow.
Parts of this work was initially presented at the *Third International Symposium on Turbulence and Shear Flow Phenomena*, Sendai, Japan, 25–27 June, 2003, where it was selected for journal publishing.

Article II:

Turbulence structures

Here, the effects of surface roughness on mainly the large scales of the turbulent incompressible flow were investigated through the examination of the higher-order statistics. It was investigated that the intensity of the vorticity fluctuations in the outer layer was unaffected by roughness. The anisotropy invariant maps for the

smooth and rough cases clearly distinguished the substantial difference in the state of turbulence near the smooth and rough walls. The turbulent transport processes in the two cases were carefully studied and it was observed that the wall-ward transport of the kinetic energy was substantially increased within the roughness sublayer while the away-from-the-wall transport of kinetic energy was relatively reduced just about the edge of the roughness sublayer.

Article III:

Budgets of Reynolds stresses

This article documents the DNS results with more focus on the Reynolds stresses. Substantial effort has gone into processing the results, in particular, Reynolds stress budgets. Through careful comparisons to a smooth- wall channel flow it was observed that roughness effects were limited to the roughness sublayer. This conclusion supported the wall-similarity hypothesis of Townsend, and as such is of definite interest to the turbulence community.
Parts of this work was presented at the *Fourth International Symposium on Turbulence, Heat and Mass Transfer*, Antalya, Turkey, 12–17 October, 2003, where it was selected for journal publishing.

Article IV:

Comparative study – Reynolds stresses

This article presents the first part of the collaborative experimental and numerical investigations in rough and smooth channels. Due to measurement and computational cost limitations, there were a relatively small Reynolds number difference between the two approaches. This articles discusses in detail, the mean velocity and Reynolds stresses variation.

Article V:

Comparative study – Further results

Further comparisons between DNS data and laboratory measurements are presented in this article. Careful study of mean velocity profile, individual components of the Reynolds stress tensor, quadrant analysis, stress ratios and Reynolds stress

anisotropy suggested that the turbulence is affected differently in the present channel flow than in rough-wall turbulent boundary layer. It was shown that the turbulence properties in the outer layer region collapse between the rough and smooth wall for both the experiments and the simulations, lending support to the wall similarity hypothesis.

References

Andreopoulos, J. & Bradshaw, P. (1981), Measurements of turbulence structure in the boundary layer on a rough surface, *Boundary-layer Meteorol.* **20**, 201–213.

Angelis, V. D., Lombardi, P. & Banerjee, S. (1997), Direct numerical simulation of turbulent flow over a wavy wall, *Physics of Fluids,* **9**, 2429–2442.

Antonia, R. A. & Krogstad, P. (2001), Turbulence structures in boundary layers over different types of surface roughness, *Fluid Dynamics Research* **28**, 139–175.

Antonia, R. A., Teitel, M., Kim, J. & Browne, L. W. B. (1992), Low-reynolds number effects in a fully developed turbulent channel flow, *Journal of Fluid Mechanics,* **236**, 579–605.

Bakken, O. M. (2004), Experimental investigation of turbulent flow in a channel with rough walls, PhD thesis, Department of Energy and Process Technology, The Norwegian University of Science and Technology.

Bandyopadhyay, P. R. (1987), Rough-wall turbulent boundary layer in the transition regime, *Journal of Fluid Mechanics,* **180**, 231–266.

Bandyopadhyay, P. & Watson, R. D. (1988), Structure of rough–wall turbulent boundary layers, *Physics of Fluids,* **31**, 1877–1883.

Barenblatt, G. I. (1999), Scaling laws for turbulent wall-boundary shear flows at very large reynolds numbers, *Journal of Engineering Mathematics* **36**, 361–384.

Bergstrom, D. J., Kotey, N. A. & Tachie, M. F. (2002), The effects of surface roughness on the mean velocity profile in a turbulent boundary layer, **124**, 664–670.

Betterman, D. (1965), Contribution a l'étude de la couche limite turbulente le long de plaque regueuses, Technical report, Centre Nat. de la Rech. Sci.

Bhaganagar, K., Kim, J. & Coleman, G. (2004), Effect of roughness on wall-bounded turbulence, *Flow, Turbulence and Combustion,* **72**(2–4), 463–492.

Cebeci, T. & Smith, A. M. (1974), *Analysis of turbulent boundary layers*, Academic Press, Inc.

Cherukat, P., Na, Y., Hanratty, T. J. & McLaughlin, J. B. (1998), Direct numerical simulation of a fully developed turbulent flow over a wavy wall, *Theoretical and Computational Fluid Dynamics* **11**, 109–134.

Chorin, A. J. (1967), A numerical method for solving incompressible viscous flow problems, *Journal of computational physics* **2**, 12–26.

Colebrook, C. F. (1938), Turbulent flow in pipes, with particular reference to the transition between the smooth and rough pipe laws, *J. Inst. Civ. Eng. Lond.* .

Darcy, H. (1857), Recherches expérimentales relatives au mouvement de léaudans les tuyaux.

Dean, R. B. & Bradshaw, P. (1976), Measurements of interacting turbulent shear layers in a duct, *Journal of Fluid Mechanics,* **78**, 641–676.

Djenidi, L., Elavarasan, R. & Antonia, R. A. (1999), The turbulent boundary layer over transverse square cavities, *Journal of Fluid Mechanics,* **395**, 271–294.

Dvorak, F. A. (1969), Calculation of turbulent boundary layers on rough surfaces in pressure gradient, *AIAA* **7**(9), 1752–1759.

Flores, O. & Jiménez, J. (2004), Effect of wall-boundary disturbances on turbulent channel flows, *in* H. I. Andersson & P.-Å. Krogstad, eds, 'Advances in Turbulence X', CIMNE, Trondheim, pp. 236–238.

Friedrich, R., Hüttl, T. J., Manhart, M. & Wagner, C. (2001), Direct numerical simulation of incompressible turbulent flows, *Computers and Fluids* **30**, 555–579.

Furuya, Y. & Fujita, H. (1967), Turbulent boundary layers on a wire-screen roughness, *Bull. JSME* .

Grass, A. J. (1971), Structural features of turbulent flow over smooth and rough boundaries, *Journal of Fluid Mechanics,* **50**, 233–255.

Grass, A. J., Stuart, R. J. & Mansour-Tehrani, M. (1993), Common vortical structure of turbulent flows over smooth and rough boundaries, *AIAA Journal* **331**, 837–447.

Grötzbach, G. (1983), Spatial resolution requirements for direct numerical simulation of the rayleigh–bénard convection, *Journal of Computational Physics* **49**, 241–264.

Hagen, G. H. L. (1854), Über den einfluss der temperatur auf die bewegung des wassers in röhren, *Math. Abh. Akad. Wiss. Berlin* .

Henn, D. S. & Sykes, R. I. (1999), Large-eddy simulation of flow over wavy surfaces, *Journal of Fluid Mechanics,* **383**, 75–112.

Hirt, C. W., Nichols, B. D. & Romero, N. C. (1975), SOLA-a numerical solution algorithm for transient fluid flows, Technical report, Los Alamos Sci. Lab.

Hodge, B. K., Taylor, R. P. & Coleman, H. W. (1989), Predicting turbulent rough-wall skin friction and heat transfer, *in* N. P. Cheremisinoff, ed., 'Encyclopedia of Fluid Mechanics', number 8, Gulf Publishing Co., Houston, London, Paris, Tokyo, chapter 13, pp. 445–468.

Jiménez, J. (2004), Turbulent flows over rough walls, *Annual Review of Fluid Mechanics* **36**, 173–196.

Johansson, P. S. & Andersson, H. I. (2004), Generation of inflow data for inhomogeneous turbulence, *Journal of Theoretical and Computational Fluid Dynamics (in press)* .

Kadanoff, L. P. (1990), Scaling and structures in the hard turbulence region of rayleigh-bénard convection, *in* L. Sirovich, ed., 'New perspectives in turbulence', Springer, p. 265.

Keirsbulck, L., Mazouz, A. & Tournier, C. (2001), Influence of the surface roughness on the third order moments of velocity fluctuations, *Experiments in Fluids,* **30**, 592–594.

Kim, J., Moin, P. & Moser, R. (1987), Turbulence statistics in fully developed channel flow at low reynolds number, *Journal of Fluid Mechanics,* **117**, 133–166.

Krogstad, P.-Å. & Antonia, R. A. (1994), Structure of turbulent boundary layers on smooth and rough walls, *Journal of Fluid Mechanics,* **277**, 1–21.

Krogstad, P.-Å. & Antonia, R. A. (1999), Surface roughness effects in turbulent boundary layers, *Experiments in Fluids,* **27**, 450–460.

Krogstad, P.-Å., Antonia, R. A. & Browne, L. W. B. (1992), Comparison between rough- and smooth-wall turbulent boundary layers, *Journal of Fluid Mechanics,* **245**, 599–617.

Leonardi, S., Orlandi, P., Smalley, R. J., Djenidi, L. & Antonia, R. A. (2003), Direct numerical simulations of turbulent channel flow with transverse square bars on one wall, *Journal of Fluid Mechanics,* **491**, 229–238.

Manhart, M. (2004), A zonal grid algorithm for DNS of turbulent boundary layers, *Computers and Fluids* **33**, 435–461.

Manhart, M. & Friedrich, R. (2002), DNS of a turbulent boundary layer with separation, *International Journal of Heat and Fluid Flow,* **23**.

Manhart, M., Tremblay, F. & Friedrich, R. (2001*a*), DNS and LES of flow around a circular cylinder at a subcritical reynolds number with cartesian grids, *in* R. Friedrich & W. Rodi, eds, 'LES of complex transitional and turbulent flows', Kluwer Academic Publishers, Dordrecht.

Manhart, M., Tremblay, F. & Friedrich, R. (2001*b*), Mglet: a parallel code for efficient DNS and LES of complex geometries, *in* , ed., 'Parallel Computational Fluid Dynamics, Trends and Applications', Elsevier Science, pp. 449–456.

Mazouz, A., Labraga, L. & Tournier, C. (1994), Behaviour of the reynolds stress on rough walls, *Experiments in Fluids,* **17**, 39–44.

Mazouz, A., Labraga, L. & Tournier, C. (1998), Anisotropy invariant of reynolds stress tensor in a duct flow and turbulent boundary layer, **120**, 280–284.

McKeon, B. J., Swanson, C. J., Zagarola, M. V., Donnelly, R. J. & Smits, A. J. (2004), Friction factors for smooth pipe flow, *Journal of Fluid Mechanics,* **511**, 41–44.

Miyake, Y., Tsujimoto, K. & Agata, Y. (2000), A DNS of a turbulent flow in a rough-wall channel using roughness elements model, *JSME International Journal* **43**, 233–242.

Miyake, Y., Tsujimoto, K. & Nakaji, M. (2001), Direct numerical simulation of rough–wall heat transfer in a turbulent channel flow, *International Journal of Heat and Fluid Flow,* **22**, 237–244.

Moody, L. F. (1944), Friction factors for pipe flow, *Trans. ASME* **66**, 671684.

Moser, R., Kim, J. & Mansour, N. (1999), Direct numerical simulation of channel flow up to $Re_\tau = 590$, *Physics of Fluids,* **11**(4), 943–945.

Nakagawa, S. & Hanratty, T. J. (2003), Influence of a wavy boundary on turbulence, II. intermediate roughened and hydraulically smooth surfaces, *Experiments in Fluids,* **35**, 437447.

Nakagawa, S., Na, Y. & Hanratty, T. J. (2003), Influence of a wavy boundary on turbulence, I. highly rough surface, *Experiments in Fluids,* **35**, 422436.

Nakayama, A. & Sakio, K. (2002), Simulation of flow over wavy boundaries, Technical report, Center for Turbulence Research.

Nieuwstadt, F. T. M. & Bradshaw, P. (1997), 'Similarities and differences of turbulent boundary-layer, pipe and channel flow'.

Nikuradse, J. (1933), Strömungsgesetze in rauhen rohren (english translation (1950): Laws of flow in rough pipes. naca tm 1292), *VDI Forschungsheft* **361**.

Perry, A. E. & Abell, C. J. (1977), Asymptotic similarity of turbulent structures in smooth– and rough–wall pipes, *Journal of Fluid Mechanics,* **79**, 785–799.

Perry, A. E., Lim, K. L. & Henbest, S. M. (1987), An experimental study of the turbulence structure in smooth- and rough-wall boundary layers, *Journal of Fluid Mechanics,* **177**, 437–466.

Perry, A. E., Schofield, W. H. & Joubert, P. N. (1969), Rough wall turbulent boundary layers, *Journal of Fluid Mechanics,* **37**, 383–413.

Prandtl, L. (1904), On the motion of a fluid with very small viscosity, *in* 'Verh. Int. Math. Kongr., 3rd, Heidelberg', pp. 484–491.

Raupach, M. R. (1981), Conditional statistics of reynolds stress in rough–wall and smooth–wall turbulent boundary layers, *Journal of Fluid Mechanics,* **108**, 363–382.

Raupach, M. R., Antonia, R. A. & Rajagopalan, S. (1991), Rough-wall turbulent boundary layers, *Applied Mechanics Review* **44**, 1–25.

Robinson, S. K. (1991), Coherent motions in the turbulent boundary layer, *Annual Review of Fluid Mechanics* **23**, 601–639.

Rouse, H. & Ince, H. (1957), *History of Hydraulics*, Iowa Satte University.

Schlichting, H. (1968), *Boundary layer theory*, 6th edn, McGraw Hill, New York.

Schultz, M. P. (2000), Turbulent boundary layers on surfaces covered with filamentous algae, **122**, 357–363.

Schumann, U. (1975), Linear stability of finite difference equations for three–dimensional flow problems, *Journal of Computational Physics* **18**, 465–470.

Shafi, H. S. & Antonia, R. A. (1995), Anisotropy of the reynolds stresses in a turbulent boundary layer on a rough wall, *Experiments in Fluids,* **18**, 213–215.

Shafi, H. S. & Antonia, R. A. (1997), Small-scale characteristics of a turbulent boundary layer flow over a rough wall, *Journal of Fluid Mechanics,* **342**, 263–293.

Smalley, R. J., Leonardi, S., Antonia, R. A., Djenidi, L. & Orlandi, P. (2002), Reynolds stress anisotropy of turbulent rough wall layers, *Experiments in Fluids,* **33**, 31–37.

Sullivan, P. P., McWilliams, J. C. & Moeng, C. (2000), Simulation of turbulent flow over idealized water waves, *Journal of Fluid Mechanics,* **404**, 47–85.

Teitel, M. & Antonia, R. A. (1990), The interaction region of a turbulent duct flow, *Physics of Fluids A* **2**(5), 808–813.

Townes, H. W. & Sabersky, R. H. (1966), Experiments of the flow over a rough surface, *International Journal of Heat and Mass Transfer* **9**, 729–738.

Townsend, A. A. (1976), *The Structure of Turbulent Shear Flow*, 2nd edn, Cambridge University Press.

Townsend, A. A. (1993), Organized eddies in turbulent shear flows, *in* J. P. Bonet & M. N. Glauser, eds, 'Eddy structure identification in free turbulent shear flows', Kluwer, Dordrecht, pp. 5–9.

Wei, T. & Willmarth, W. W. (1989), Reynolds number effects on a structure of a turbulent channel flow, *Journal of Fluid Mechanics,* **204**, 57–95.

Werner, H. (1991), Grobstruktursimulation der turbulenten Strömung über eine querliegende Rippe in einem Plattenkanal bei hoher Reynoldszahl, PhD thesis, Lehrstuhl für Strömnungsmechanik, Technische Universität München, Germany.

White, F. M. (1999), *Fluid Mechanics*, 4th edn, McGraw Hill.